GSA Data Repository 2019087

Incel, S., et al., 2019, Reaction-induced embrittlement of the lower continental crust: Geology, https://doi.org/10.1130/G45527.1

1 STRESS AND STRAIN CALCULATION

To monitor the strain during deformation gold foils that acted as strain markers in X-ray radiographs were placed at the bottom and the top of the sample. The powder diffraction patterns gave access to the differential stresses sustained by lattice planes of a certain phase due to the distortion of the Debye rings in an anisotropic stress field. Hilairet et al., (2012) give further details on the strain and stress calculation. These differential stresses were calculated on the (-201), (111), (002), and the (-220) lattice planes of plagioclase using available elasticity data (Brown et al., 2006) and thermal expansion coefficients (Tribaudino et al., 2010) from literature. The mean stresses of each experiment were re-calculated using the average of the differential stress on the (002) and the (111) lattice planes of plagioclase and the confining pressure (P_c). The confining pressures (see the table in Fig. 1) were estimated using the peak shift in the diffraction pattern taken at ambient conditions and after pressurization and heating. Because calculating stress using triclinic symmetry did not lead to reliable results, the calculation was performed with orthorhombic crystal symmetry. Prior to deformation, the powder samples were hot-pressed in-situ, at their respective confining pressures and their minimum temperatures (table in Fig. 1). After hot-pressing the samples for around one hour, deformation started at a controlled constant strain rate of $\sim 5 \cdot 10^{-5}$ s^{-1}.

2 ANALYTICAL METHODS

All samples were investigated using the Zeiss Sigma field-emission scanning electron microscope (FE-SEM) at Ecole Normale Supérieure, Paris. Backscattered electron (BSE)

images were acquired with an acceleration voltage of 15 kV. For the energy-dispersive X-ray spectroscopy (EDS) element distribution maps, the acceleration voltage was lowered to 10 kV to obtain a higher resolution. The electron backscatter diffraction (EBSD) analyses were performed using an Oxford instruments EBSD detector installed on the same SEM at Ecole Normale Supérieure Paris. Analyses were conducted at an acceleration voltage of 15 kV and the EBSD data was generated using the Oxford Instruments AZtecHKL EBSD system. To investigate the nanostructure, a focused ion beam (FIB) section was cut using a FEI Strata DB 235 at IEMN at the University of Lille, France. The transmission electron microscopy (TEM) analyses were performed on a JEM 2011 at the Laboratoire de Réactivité de Surface at Université Pierre et Marie Curie Paris, France. The TEM images were taken in bright field (BF) mode with an acceleration voltage of 200 kV.

3 CALCULATION OF E_a (EXPLANATIONS TO FIGURE 4)

To calculate the activation energy E_a, an Avrami type equation (Poirier, 1982)

$$X(t) = 1 - \exp(-kt^n) \quad (1)$$

was used, with X, the advancement of reaction, t, the time in seconds, and k the kinetics factor that can be written as an Arrhenius function

$$k = k_0 \times \exp(-E_a/RT), \quad (2)$$

where E_a is the activation energy term, R the gas constant and T the temperature in K. Assuming n=1 for nucleation at grain boundaries (Cahn, 1956), equations (1) and (2) derive into:

$$ln(X(t)) = k_0 \times \exp(-E_a/RT) \times t. \quad (3)$$

where X is the reacted granulite volume over t the finite duration of the experiments and is measured from microstructural observations. Considering that dX/dt, the instantaneous reaction rate is constant over the short duration of our experiments yields:

$$ln(X/(1-X))/t = k_0 \times \exp(-E_a/RT), \quad (4)$$

For the two experiments performed at constant temperature, NG_2.5_1023 and NG_2.5_1173, we plotted ln k_0 over $1/(RT)$. The slope of the regression line between these two points is the activation energy with $E_a \approx 215$ kJ·mol^{-1}. However, the reacted volumes cannot be estimated precisely and any change would affect the slope. The exact determination of E_a for anorthite breakdown in the presence of fluid exceeds the scope of the present study and since it lies in the same order of magnitude as E_a for other known transitions, e.g. 162 kJ·mol^{-1} for the quartz-coesite (Perrillat et al., 2003) and 259 kJ·mol^{-1} for the olivine-spinel transition (Poirier, 1981), we consider that for our purpose the calculated E_a represents a reasonable estimate of the activation energy.

Brown, J.M., Abramson, E.H., and Angel, R.J., 2006, Triclinic elastic constants for low albite: Physics and Chemistry of Minerals, v. 33, p. 256–265, doi: 10.1007/s00269-006-0074-1.

Cahn, J.W., 1956, The kinetics of grain boundary nucleated reactions: Acta Metallurgica, v. 4, p. 449–459, doi: 10.1016/0001-6160(56)90041-4.

Hilairet, N., Wang, Y., Sanehira, T., Merkel, S., and Mei, S., 2012, Deformation of olivine under mantle conditions: An in situ high-pressure, high-temperature study using monochromatic synchrotron radiation: Journal of Geophysical Research: Solid Earth, v. 117, p. 1–16, doi: 10.1029/2011JB008498.

Perrillat, J.P., Daniel, I., Lardeaux, J.M., and Cardon, H., 2003, Kinetics of the Coesite–Quartz Transition: Application to the Exhumation of Ultrahigh-Pressure Rocks: Journal of Petrology, v. 44, p. 773–788, doi: 10.1093/petrology/44.4.773.

Poirier, J.P., 1981, On the kinetics of olivine-spinel transition: Physics of the Earth and Planetary Interiors, v. 26, p. 179–187, doi: 10.1016/0031-9201(81)90006-6.

Poirier, J.P., 1982, On transformation plasticity: Journal of Geophysical Research, v. 87, p. 6791–6797.

Tribaudino, M., Angel, R.J., Cámara, F., Nestola, F., Pasqual, D., and Margiolaki, I., 2010, Thermal expansion of plagioclase feldspars: Contributions to Mineralogy and Petrology, v. 160, p. 899–908, doi: 10.1007/s00410-010-0513-3.

Fig. DR1

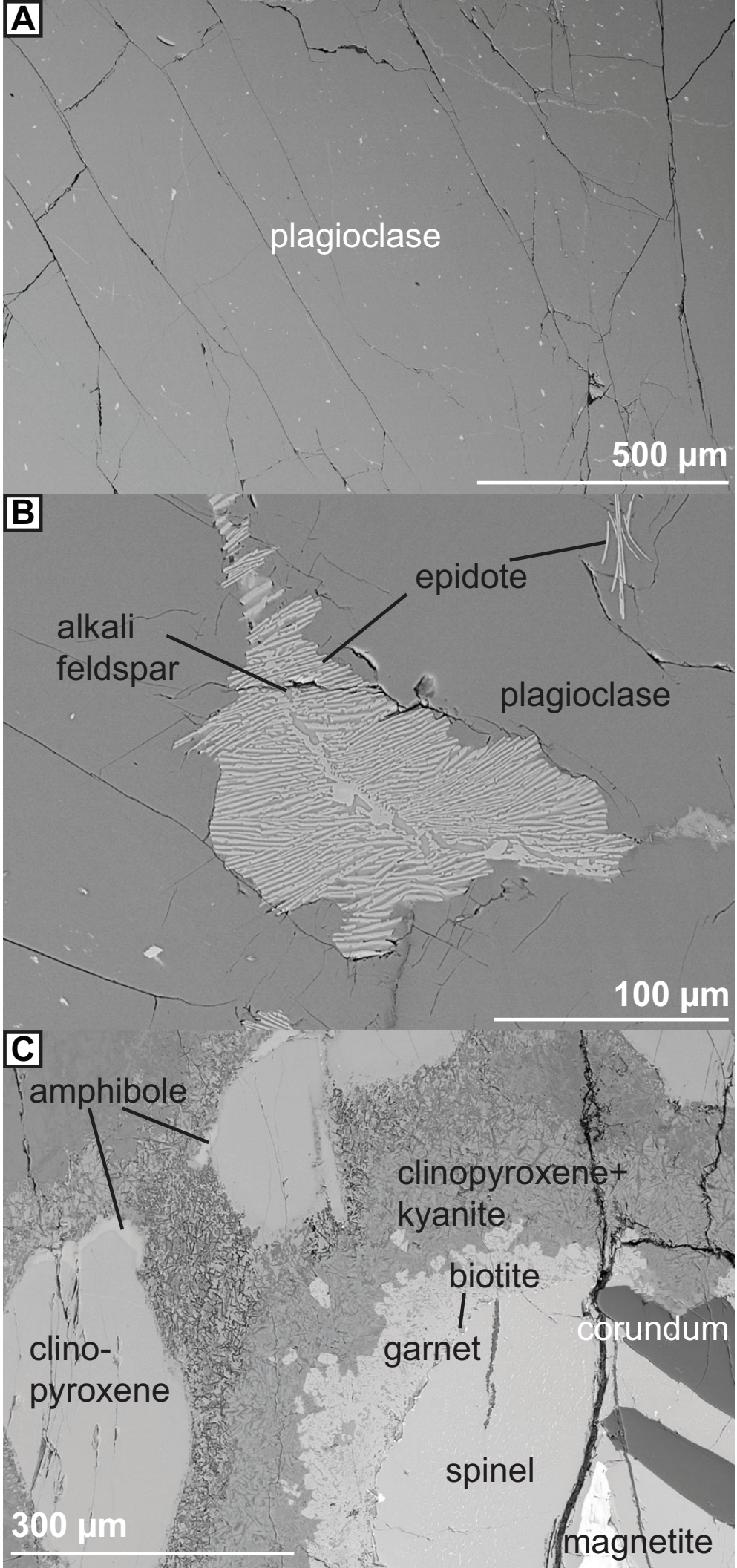
A
plagioclase
500 µm
B
epidote
alkali
feldspar
plagioclase
100 µm
C
amphibole
clinopyroxene+
kyanite
biotite
corundum
garnet
clino-
pyroxene
spinel
300 µm
magnetite

Fig. DR2

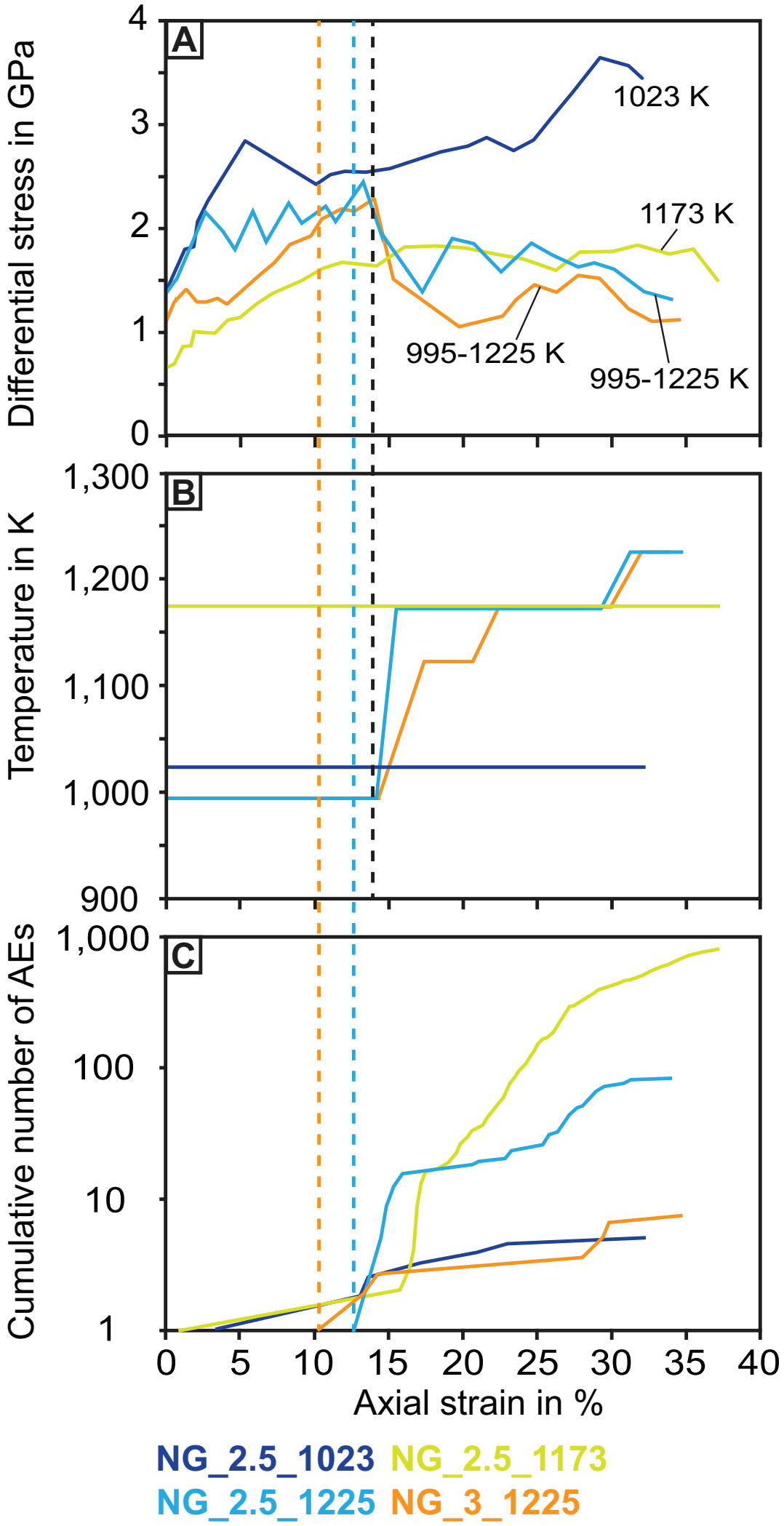
A
B
C
Differential stress in GPa
Temperature in K
Cumulative number of AEs
Axial strain in %
1023 K
1173 K
995-1225 K
995-1225 K
0
1
2
3
4
900
1,000
1,100
1,200
1,300
1
10
100
1,000
0
5
10
15
20
25
30
35
40
NG_2.5_1023
NG_2.5_1173
NG_2.5_1225
NG_3_1225

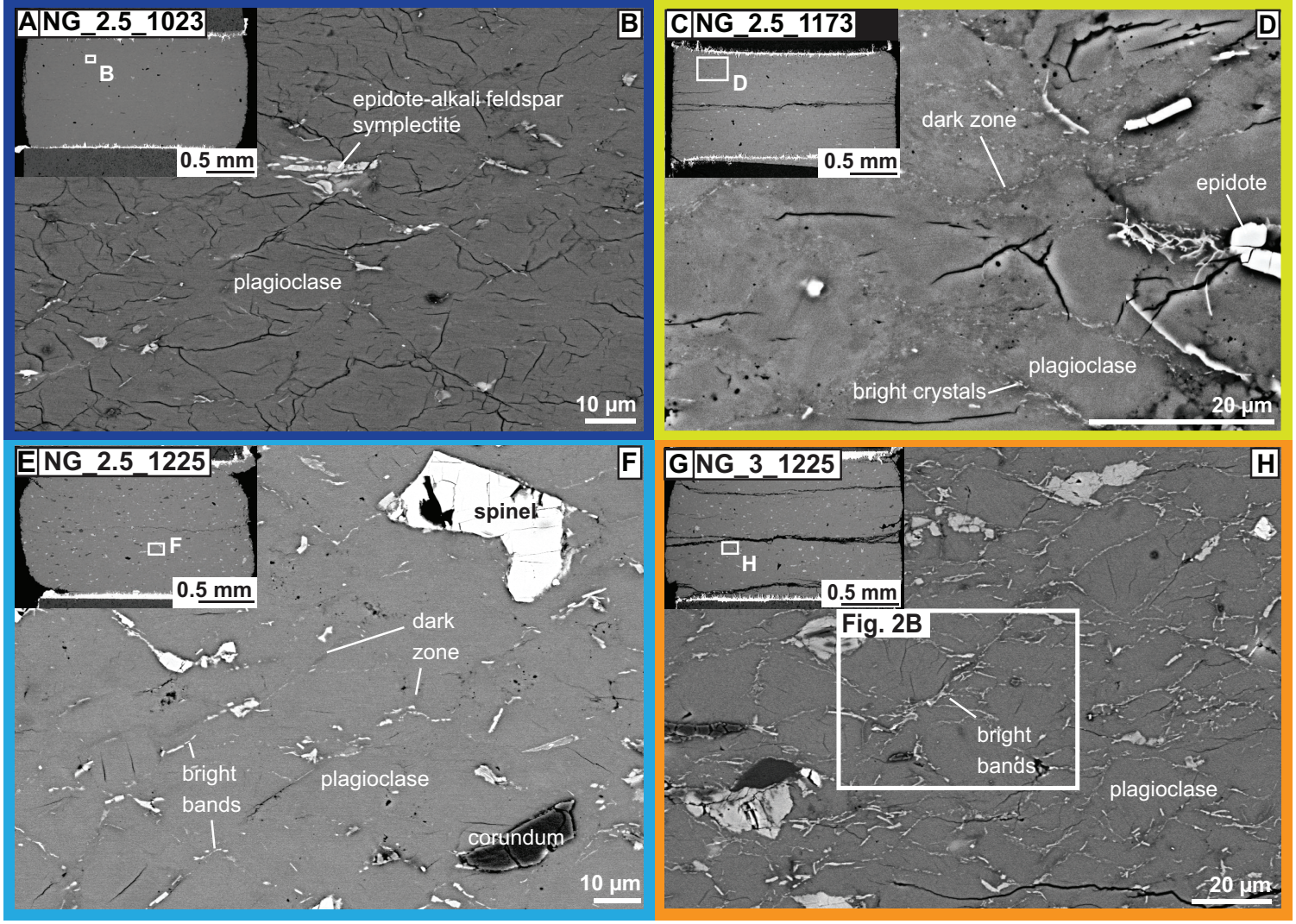
A NG_2.5_1023
B
0.5 mm
B
epidote-alkali feldspar
symplectite
plagioclase
10 µm
C NG_2.5_1173
D
0.5 mm
D
dark zone
epidote
plagioclase
bright crystals
20 µm
E NG_2.5_1225
F
0.5 mm
F
spinel
dark
zone
bright
bands
plagioclase
corundum
10 µm
G NG_3_1225
H
0.5 mm
H
Fig. 2B
bright
bands
plagioclase
20 µm

Fig. DR3

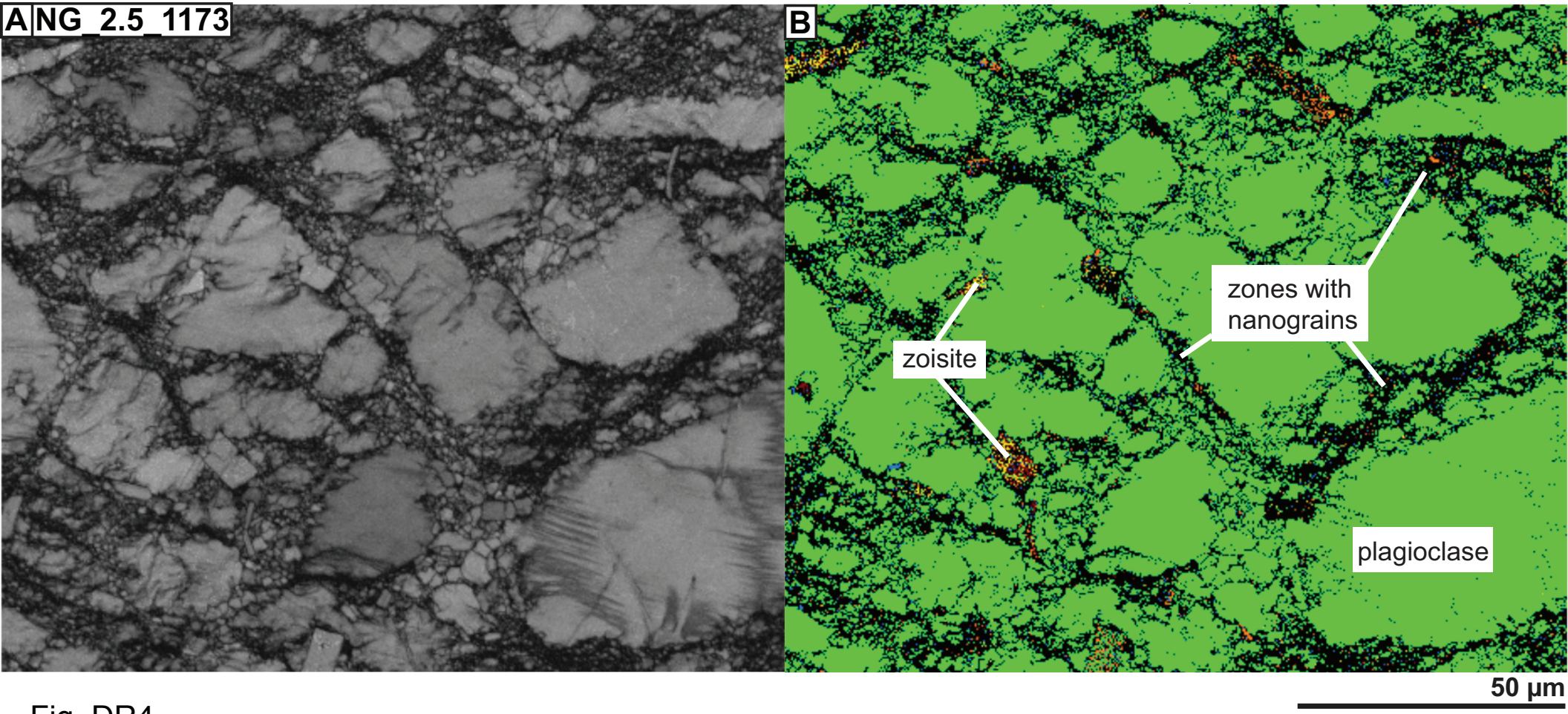
A
NG_2.5_1173
B
zoisite
zones with
nanograins
plagioclase
50 µm

Fig. DR4

Fig. DR5

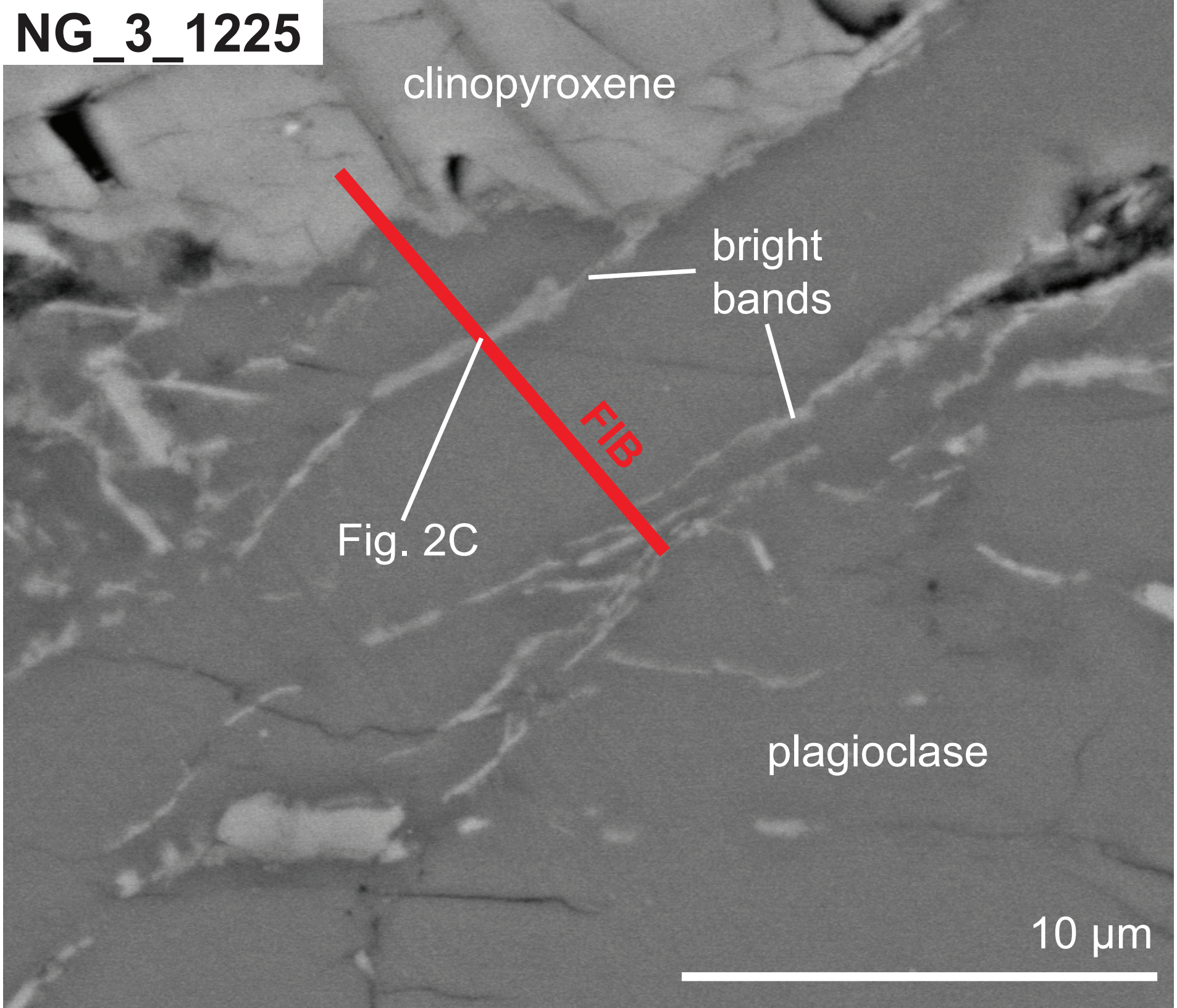
NG_3_1225
clinopyroxene
bright bands
FIB
Fig. 2C
plagioclase
10 µm